Research Article Vol. 29, No. 2 / 18 January 2021 / Optics Express 821
Optics EXPRESS

Automatic, high-speed, high-precision acquisition scheme with QPD for the Taiji program

RUIHONG GAO,[1,2,3] HESHAN LIU,[1] YA ZHAO,[2,4] ZIREN LUO,[1,*] AND GANG JIN[1,2]

[1]Institute of Mechanics, Chinese Academy of Sciences, Beijing 100190, China
[2]School of Engineering Science, University of Chinese Academy of Sciences, Beijing 100049, China
[3]School of Fundamental Physics and Mathematical Sciences, Hangzhou Institute for Advanced Study, University of Chinese Academy of Sciences, Hangzhou 310024, China
[4]Changchun Institute of Optics, Fine Mechanics and Physics, Chinese Academy of Sciences, Changchun 130033, China
*luoziren@imech.ac.cn

Abstract: Most of the space gravitational wave detection missions, such as the Taiji program, use space-based laser interferometer to sense the gravitational waves. However, to obtain the interference signal, the inter-satellite laser acquisition scheme is firstly required to establish the laser link. Traditional acquisition sensors are CCD cameras, which cause a serious heating problem and call for high alignment precision. To avoid these questions, a high-speed, high-precision, fully automatic acquisition scheme with quadrant photodetectors (QPD) is proposed in this paper. Incoherent measurement method of the QPD is introduced to fulfill high-speed acquisition, while a dedicated imaging system is involved for automatic acquisition. Also, an improved differential power sensing (DPS) signal is developed. Combined with the down-sampling algorithm and the match filter algorithm, the acquisition scheme can achieve 1 μrad resolution with total scanning time less than 220 s.

1. Introduction

The American ground-based gravitational wave detector (LIGO) announced the first direct detection of gravitational waves in 2016 [1]. The exciting news promoted the development of the space-based gravitational wave detection missions such as the LISA [2] and the Taiji program [3–6]. After comparing various schemes, such as atomic interference, cold atomic clock and quantum light source [7], laser interferometer is chosen as the final scheme of the LISA [8], the Taiji [3–6] and the Tianqian [9]. Because of the long distance between two satellites as well as the limited navigation precision, the interference signal can only be obtained after a complicated process called laser signal acquisition. For the Taiji program, the deviation angle should be suppressed from about 1 mrad to 1 μrad with the help of an acquisition system. Because of the finite precision of star-trackers (STRs) which can only suppressed the deviation angle to 10 μrad magnitude, other acquisition sensors are also required. It is also required that the influence of the acquisition system to the science interferometer system should be as small as possible while the scanning time should also be small enough to reduce the risk of alignment failure [10]. On the other hand, considering the far distance of about ten million between the satellites and the Earth, the whole process should be accomplished automatically for saving resources of upload and download.

The preliminary design of the acquisition scheme adopts CCD or CMOS camera as one of the acquisition sensors [10]. With the help of a dedicated scanning scheme, the CCD cameras of each satellite will receive the laser beam from the opposite satellite at a certain time. Then

#408822 https://doi.org/10.1364/OE.408822
Journal © 2021 Received 1 Sep 2020; revised 16 Dec 2020; accepted 17 Dec 2020; published 5 Jan 2021

Optics EXPRESS

the attitude of the satellites can be adjusted by comparing the position of the laser spot with a reference position. To maintain a stable thermal environment, no cooling devices will be used on the optical bench of the Taiji. As a result, although the CCD has high resolution, it has serious heating problem. Based on the technical discussion of the LISA pathfinder [11], the heating problem of the colloid thrusters outside the satellite will deteriorate the measuring precision of the interferometer to ten nanometer magnitude. Only by closing the thruster for two weeks, can the precision return to few picometer magnitude. Similarly, the heating problem of the CCD will cause the same problem. To maintain the orbit stability and optimize the relative velocity between the satellites, the orbit has to be adjusted frequently. During the adjustment phase, whenever the laser link loses lock, the acquisition process needs to be operated again. Then, the science interferometer can only return to normal operation after standing a few weeks. It is a large waste of time of science data collecting. On the other hand, the alignment accuracy between the acquisition system and the interferometry system need to reach 10 μrad magnitude, which brings difficulty to assemble.

Because of the above deficiencies, the Quadrant Photodetector (QPD) of the science interferometer are considered to be used as the acquisition sensor [12]. As the QPD is the detector for the interferometer itself, both the heating problem and the assembly problem will not exist anymore. If an automatic acquisition scheme only with QPDs is well designed, the CCD will no longer be used, which reduces costs as well. As a result, some QPD direct acquisition schemes have been tried on the GRACE Follow-on mission [12]. The first generation QPD automatic acquisition scheme adopts the interference signal of the local beam and the receiving beam as the acquisition signal. Within the field of view of 1.4 mrad, the acquisition precision reaches 100 μrad [13,14]. However, the scanning time is as long as six hours. Therefore, in the second generation, random scan mode is involved. The scanning time reduces to one hour. But it still needs six hours when we consider the satellite attitude disturbance [15]. In the third generation, incoherent measurement is used. The scanning time reduces to 160 s by decoupling the acquisition degrees of freedom, while the acquisition precision increases to 35 μrad [16]. However, this scheme needs data transmission between satellites and ground. As a result, the automatic acquisition process, which is required by the Taiji/LISA program, cannot be fulfilled.

In summary, an automatic, high-speed, high-precision acquisition scheme with QPD is essential to the gravitational wave detection missions. In this paper, we present such acquisition scheme. For fulfilling automatic acquisition, the QPD incoherent measurement method as well as a dedicated imaging system is adopted. We also develop an improved differential power sensing (DPS) signal to improve the capability of recognition to the weak signal. On the other hand, a down-sampling algorithm and the match filter algorithm are used to improve the acquisition precision. According to the simulation results, the automatic acquisition precision of 1 μrad can be fulfilled within 220 s.

2. Acquisition method

2.1. Strategies for QPD Automatic Acquisition

In the acquisition phase, the two satellites are denoted as master satellite and slave satellite respectively (as shown in Fig. 1). Based on the navigation data and the STR data, the two satellites achieve their initial line of sight (LOS). The angular offset between initial LOS_m and the real direction is φ_m, while the angular offset between initial LOS_s and the reference LOS is φ_s, where reference LOS is parallel to initial LOS_{master}. During the master scanning, φ_m can be used to indicate the position of the slave satellite with respect to the master satellite while φ_s can be used to represent the pointing direction of the slave satellite. φ_m and φ_s can be orthogonal decomposed to ($\varphi_{m,yaw}$, $\varphi_{m,pitch}$) and ($\varphi_{s,yaw}$, $\varphi_{s,pitch}$). Therefore, the laser incident angle of the slave satellite can be denoted as ($\varphi_{m,yaw}$-$\varphi_{s,yaw}$, $\varphi_{m,pitch}$-$\varphi_{s,pitch}$).

Optics EXPRESS

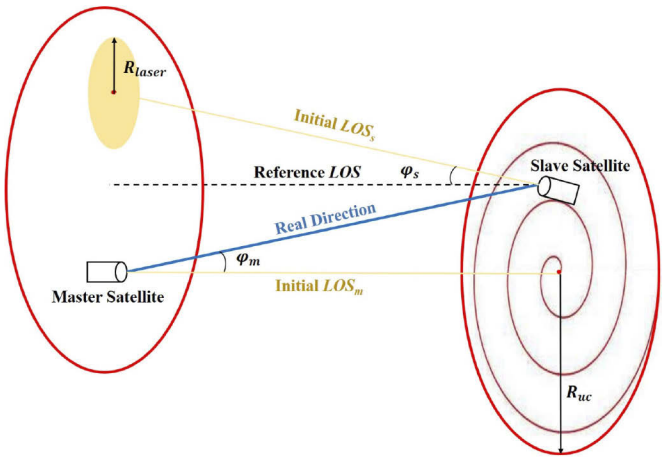

Fig. 1. Schematic diagram of laser acquisition. Where, initial LOS_m and initial LOS_s are the initial line of sight of the master satellite and the slave satellite respectively, real direction is the correct direction with no angular offset, reference LOS is parallel to Initial LOS_m. φ_m and φ_s represent the angular offset, R_{uc} is the radius of the uncertainty zone, R_{laser} is the radius of the laser spot.

For realizing QPD automatic acquisition, we involve a dedicated imaging system similar with the one used in CCD acquisition stage of the preliminary Taiji acquisition scheme. Then, the scanning process of our scheme is introduced as follows. At first, the slave satellite stares into its initial direction while the master satellite scans over the whole area where the slave satellite may exist. This area is called uncertainty zone. At a certain time, the QPD on the slave satellite can receive the laser with enough power. With the help of the imaging system, the laser spot images to different positions on QPD surface. The offset of the laser spot from the QPD center is proportion to the incident angle in the corresponding direction while the offset value can be distinguished by the detected signal of the four quadrants. After processing the data of the four quadrants, the slave satellite can adjust its attitude and stares into the direction of the master satellite automatically. Then the QPD on the master satellite will also receive a laser beam. Similarly, the attitude of the mater satellite can also be adjusted automatically.

For the Taiji program, the angle of the scanning uncertainty zone after STR coarse pointing is approximate ±23.9 μrad, while the laser divergence angle is about ±1.43 μrad. Correspondingly, the scanning uncertainty radius (R_{uc}) is 75 km and the radius of the far-field laser spot (R_{laser}) is 4.3 km. The scanning pattern of our scheme is the constant tangential speed Archimedean spiral. It is presented in Fig. 2. Compared with other scanning patterns, such as Lissajous patterns, it can cover the scanning area uniformly. The mathematical description of the spiral can be given by,

$$\overrightarrow{r} = \frac{d}{2\pi}\varphi(t)\begin{pmatrix}\cos\varphi(t)\\ \sin\varphi(t)\end{pmatrix}, \quad \text{where} \quad \varphi(t) = 2\pi\frac{r_{\max}}{d}\sqrt{\frac{t}{T}}, \tag{1}$$

where, r_{max} is the maximum value of the spiral radius, T is the total scanning time and d is the arc separation.

With the help of the dedicated imaging system, whenever the laser beam projects on the QPD surface, the incident angle can be derived from the position of the laser spot. We suppose that the incident angles of the yaw and the pitch direction are θ_{yaw} and θ_{pitch} respectively. The laser spot offset on the QPD surface can be written as,

$$r_{ud} = k_{ud}\cdot\theta_{pitch}, \quad r_{rl} = k_{rl}\cdot\theta_{yaw}, \tag{2}$$

Optics EXPRESS

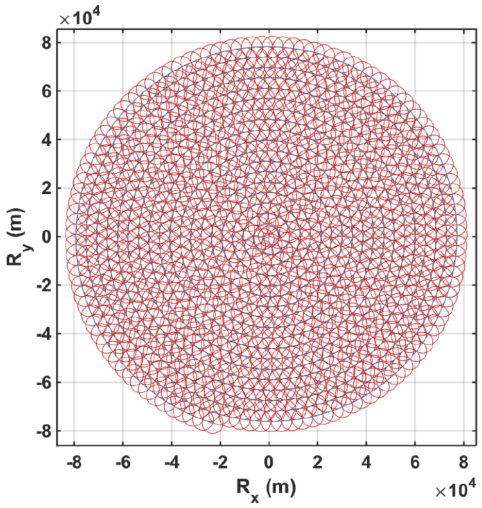

Fig. 2. The constant tangential speed Archimedean spiral scanning pattern used in the QPD acquisition scheme.

where, k_{ud} and k_{rl} are the scale factor of the imaging system, r_{ud} and r_{rl} are the offset in the y-direction and the x-direction of the QPD surface respectively. The diagram is shown in Fig. 3.

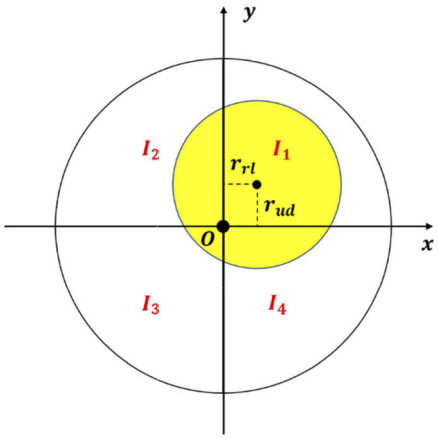

Fig. 3. The diagram of the QPD surface with a laser spot.

Traditionally, the offset value can be obtained from the detected data of the four quadrants with the differential power sensing technique (DPS) [17], which is given by,

$$DPS_{rl} = \frac{I_1 + I_4 - (I_2 + I_3)}{I_1 + I_2 + I_3 + I_4}, \quad DPS_{ud} = \frac{I_1 + I_2 - (I_3 + I_4)}{I_1 + I_2 + I_3 + I_4}, \tag{3}$$

where I_1, I_2, I_3 and I_4 represent the current (voltage) of each quadrant. It has been proved that the DPS signal is proportion to the offset value within certain range [18]. However, the DPS signal is sensitive to noise because it equals to zero when the laser spot is around the QPD center. Therefore, we develop an improved DPS signal as,

$$D_{rl} = \frac{I_1 + I_4}{I_1 + I_2 + I_3 + I_4}, \quad D_{ud} = \frac{I_1 + I_2}{I_1 + I_2 + I_3 + I_4}. \tag{4}$$

Optics EXPRESS

We consider the right and left quadrants as an example. Based on simulation, we obtain the relationship between the offset length r and D_{rl} (as shown in Fig. 4). From Fig. 4, we can conclude that the proportional relationship between r_{rl} and D_{rl} is still valid when the offset length is small. The nonlinear property increases with the offset length. This is mainly due to the fact that some part of the laser spot moves beyond the boundary of the detector when the offset increases. As the value of D_{rl} equals to 0.5 in the center, the weight of the position detection signal is larger than that of the traditional DPS signal. As a result, in theory, the improved DPS signal is less sensitive to noise when the spot is near the center.

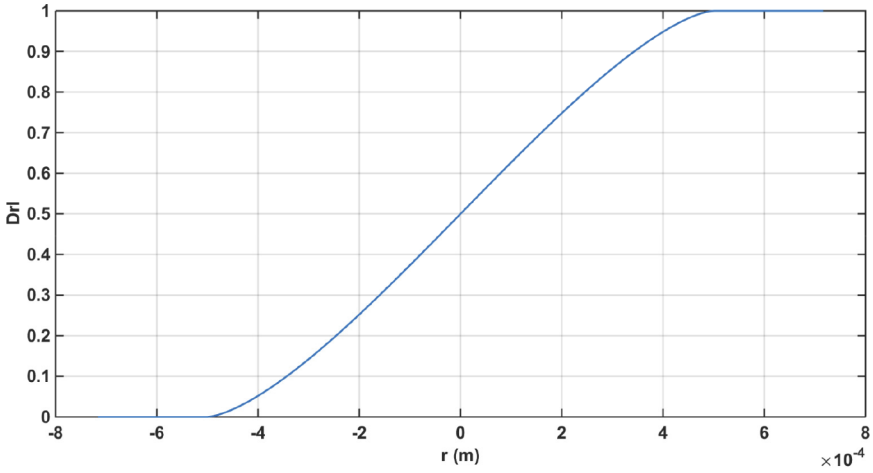

Fig. 4. The relationship between D_{rl} and the offset length r in the horizontal direction. In the simulation, the diameter of the QPD is set to 1 mm while the diameter of the laser spot is 0.5 mm. At this time, the linear fitting coefficient q_{rl}= q_{ud}≈2533 /m.

Suppose the linear fitting coefficient of D_{rl} and D_{ud} are q_{rl} and q_{ud} respectively. Within the linear portion, the incident angles can be given by,

$$\theta_{yaw} = \frac{D_{rl} - 0.5}{q_{rl} \cdot k_{rl}}, \quad \theta_{pitch} = \frac{D_{ud} - 0.5}{q_{ud} \cdot k_{ud}}. \tag{5}$$

Then, the angles can be used to adjust the attitude of the satellites for realizing automatic acquisition.

2.2. Strategies for QPD high-speed acquisition

As the distance between the two satellites of the Taiji is about three million kilometers, the receiving laser power of one quadrant of the QPD is as weak as 100 pW magnitude. For the photoelectric conversion efficiency of 0.7, the amplitude of the photocurrent is of 70 pA magnitude. On the other hand, the detected data also includes the equivalent current noise (ECN) of the QPD. The amplitude spectral density (ASD) of the Taiji QPD ECN is about 1.5 pA/$\sqrt{\text{Hz}}$[19,20]. With the sampling frequency of 50 MHz, the current noise could be 10 nA magnitude (as shown in Fig. 5(a) for the Gaussian white noise), which is far larger than the photocurrent. The signal current is completely submerged in noise with QPD direct light intensity detection methods (like DPS technique). However, just as the science measurement process of the Taiji, the QPD works well within its measurement bandwidth (1 MHz – 25 MHz) for detecting interference signal. Therefore, using the AC signal is a better choice in QPD acquisition under weak receiving light conditions.

To obtain the signal within the QPD bandwidth, traditional methods make the laser operate frequency scan. As a result, spatial degrees of freedom are coupled with the frequency scanning

Optics EXPRESS

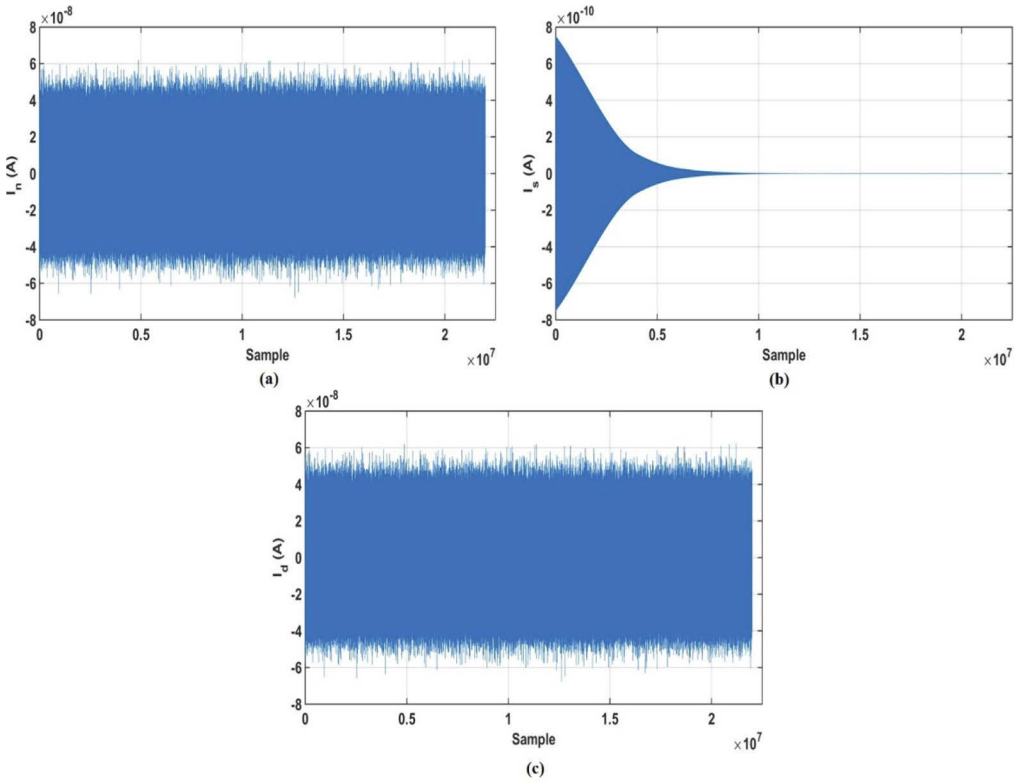

Fig. 5. With the sampling frequency of 50 MHz, the stepping time of 0.04 s, the simulation curve of (a) Noise current (b) Photo current (c) Combination of noise and signal within the whole scanning.

degree of freedom. It will greatly increase the whole scanning time. Therefore, the incoherent measurement method is used in our QPD automatic acquisition scheme. Since the bandwidth of the QPD used in the Taiji program is 1 MHz – 25 MHz, a resonant electro–optical amplitude modulator is put behind each laser to modulate the laser power at a frequency within such bandwidth. The local photodetector can detect the laser signal whenever the transmitted laser beam reaches the receiving satellite. The power of the laser beam after modulation P can be written as,

$$P(t) = \frac{1}{2}P_0[1 + \cos(2\pi ft)], \tag{6}$$

where, f is the power modulation frequency, P_0 is the power of the laser beam.

2.3. Strategies for QPD high-precision acquisition

We suppose that the remote satellite in located in the center of the uncertainty cone and the stepping time is $0.04s$. With the incoherent measurement method, the modulated laser signal is shown in Fig. 5(b). When we combine Fig. 5(a) and Fig. 5(b), we find that the signal current is still submerged in noise from Fig. 5(c). Therefore, we consider adopting a narrow band-pass filter to solve the problem.

On the other hand, the received signal is sampled by an analog-digital convertor (ADC). As the modulation frequency is as high as 1 MHz magnitude, high sampling frequency is required. We suppose that the modulation frequency is 25 MHz and the sampling frequency is 50 MHz. Suppose the scanning time is 100 s, the amount of data is as big as 60 Gbit with a 12-bit ADC.

Optics EXPRESS

Such large amount of data will bring a lot of problems in storage and post-processing. In order to reduce the amount of effective data as well as improve the signal to noise ratio (SNR), the single frequency discrete Fourier transform algorithm is used. The down-sampling algorithm works like a narrow band-pass filter as well. We chop the total scanning time T into thousands of segments whose time duration is T_{ch}. Then the number of segments N equals to $T/\ T_{ch}$. The description of the ith (i=1, 2, . . . , N) down-sampling data of the jth (j=1, 2, 3, 4) quadrant ($s_{i,j}$) is presented as follows,

$$x_j = \sum_{n\cdot\Delta t=(i-1)\cdot T_{ch}}^{i\cdot T_{ch}-\Delta t} S_j(n\cdot\Delta t)\cdot\sin(2\pi fn\cdot\Delta t) \tag{7}$$

$$y_j = \sum_{n\cdot\Delta t=(i-1)\cdot T_{ch}}^{i\cdot T_{ch}-\Delta t} S_j(n\cdot\Delta t)\cdot\cos(2\pi fn\cdot\Delta t) \tag{8}$$

$$s_{i,j} = \sqrt{x_j^2 + y_j^2}, \tag{9}$$

where, Δt=1/f_s denotes the sampling time, S_j (n·Δt) (n=0, 1, 2, . . .) is the data of the jth quadrant sampled by the ADC. After down-sampling, the overall data detected by the QPD is written as,

$$S_{i,all} = s_{i,1} + s_{i,2} + s_{i,3} + s_{i,4} \tag{10}$$

The down-sampling data is substitute for the current in the formula (4). Then the value of D_{rl} and D_{ud} can be rewritten as,

$$D_{i,rl} = \frac{s_{i,1} + s_{i,4}}{s_{i,1} + s_{i,2} + s_{i,3} + s_{i,4}}, \quad D_{i,ud} = \frac{s_{i,1} + s_{i,2}}{s_{i,1} + s_{i,2} + s_{i,3} + s_{i,4}}. \tag{11}$$

To improve the SNR, together with the down-sampling algorithm, the match filter algorithm is also introduced. When the master satellite scans, the slave satellite may be anywhere within the uncertainty zone. We suppose that the angle range in the horizontal and the vertical direction of the uncertainty zone is from -θ_{uc} to +θ_{uc}. We grid these two directions with a gridding size of θ_g. Then there will be $(\frac{2\theta_{uc}}{\theta_g} + 1)^2$ gridded positions for the slave satellite. At each position, the QPD on the slave satellite will receive the laser signal at different time. For the mth (m=1, 2, . . . , $(\frac{2\theta_{uc}}{\theta_g} + 1)^2$) position, we can pre-calculate $S_{i,all}$ without considering noises. The result is denoted as $T^m_{i,all}$. The template bank is saved as a data base on the slave satellite. Then, after down-sampling processing, the received noisy data will be match filtered by the templates. We calculate a simple correlation function as defined below,

$$C_m = \sum_{i=1}^{N} S_{i,all}\cdot T^m_{i,all}. \tag{12}$$

The template $T^{m_{\max}}_{i,all}$, which gives the maximum value of C_m, is selected as the position of the slave satellite related to the master satellite. Then, the maximum down-sampling data $T^{m_{\max}}_{i_{\max},all}$ of the m_{max}th template is retrieved. The i_{max}th down-sampling data related to the moment when the QPD receives the maximum laser power. At this time, D_{rl} and D_{ud} has the best SNR. With the help of the imaging system, the position of the master satellite related to the slave satellite can be calculated by substituting $D_{i_{\max},rl}$ and $D_{i_{\max},ud}$ into formula (5). Based on the following result, the slave satellite can adjust its attitude and point to the master satellite. Similarly, the master satellite can operate the same process after receiving the laser signal from the slave satellite.

Optics EXPRESS

2.4. Summary

In this section, we present the strategies used in the automatic QPD acquisition scheme. For fulfilling automatic acquisition, a dedicated imaging system is involved. Incoherent measurement method is also used to decouple frequency and spatial scan, which can greatly decrease the scanning time. Noises, especially the equivalent current noise, influence the acquisition precision a lot. We use the down-sampling algorithm as well as the match filter algorithm to improve SNR. We also develop an improved DPS signal which is less sensitive to noise. In section 3, the performance of the automatic QPD direct acquisition method is presented based on numerical simulation.

3. Results and discussion

In this section, we verify the applicability of the automatic QPD acquisition scheme to the Taiji program via experiment and numerical simulation.

3.1. Verification of adaptivity of the improved DPS signal

In section 2.1, we present the improved DPS signal as formula (4). To verify the linearity performance and the anti-noise performance of D_{rl} and D_{ud}, we establish an experiment system (as shown in Fig. 6). Here, the attenuator is used to change laser intensity, the steering mirror is used to change the laser spot position on the QPD surface and the beam expander is used to adjust the size of the laser spot for adapting to the QPD size.

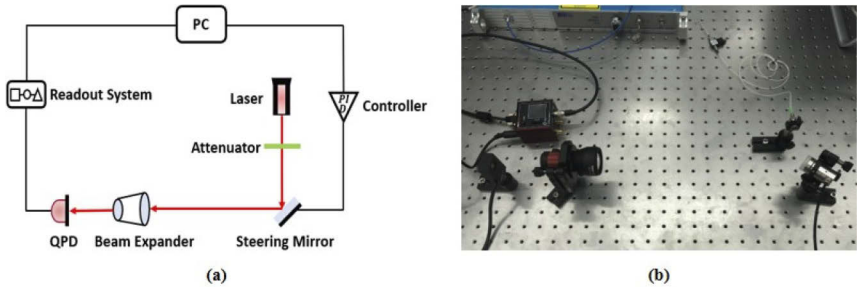

Fig. 6. The experiment system for verifying the performance of the improved DPS. (a) Schematic diagram. (b) Physical diagram.

By adjusting the deflection angle of the steering mirror, we can change the offset length of the laser spot on the QPD surface and detect the improved DPS signal and traditional DPS signal. However, the rotation axes can hardly be placed parallel or perpendicular to the optical bench, as shown in Fig. 7. (x_Q, y_Q, z_Q) represents the coordinate that parallels to the QPD coordinate, (x_r, y_r, z_r) represents the rotation coordinate, where x_r, y_r denote the rotation axes of the steering mirror and z_r coincides with z_Q. When we change the deflection angle of the steering mirror of one axis (x_r or y_r), the offset length in both x_Q and y_Q direction will change on the QPD surface because of the existence of the included angle between the two coordinates (θ). Therefore, it is of great importance to obtain the relationship between the rotation angle of the steering mirror and the offset length on the QPD surface first.

To simplify the calculation, we suppose that the steering mirror is only controlled to rotate around the y_r axis. The following results are also applicable to the rotation around the x_r axis. The rotation angle is denoted as α. After rotating angle α around y_r, (x_Q, y_Q, z_Q) and (x_r, y_r, z_r) are reformulated as (x'_Q, y'_Q, z'_Q) and (x'_r, y'_r, z'_r) respectively. The coordinate transfer

Optics EXPRESS

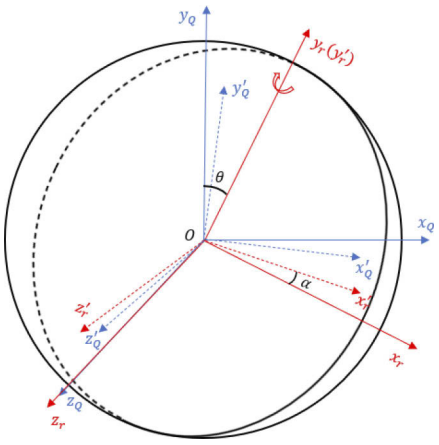

Fig. 7. The diagram of the coordinates of the steering mirror. Where, (x_Q, y_Q, z_Q) represents the coordinate that parallels to the QPD coordinate, (x_r, y_r, z_r) represents the rotation coordinate. After rotating angle α around y_r, (x_Q, y_Q, z_Q) and (x_r, y_r, z_r) are reformulated as (x'_Q, y'_Q, z'_Q) and (x'_r, y'_r, z'_r) respectively.

matrices of the coordinates can be denoted as,

$$\begin{pmatrix} x'_r \\ y'_r \\ z'_r \end{pmatrix} = \begin{pmatrix} \cos\alpha & 0 & \sin\alpha \\ 0 & 1 & 0 \\ -\sin\alpha & 0 & \cos\alpha \end{pmatrix} \cdot \begin{pmatrix} x_r \\ y_r \\ z_r \end{pmatrix} \tag{13}$$

$$\begin{pmatrix} x'_Q \\ y'_Q \\ z'_Q \end{pmatrix} = \begin{pmatrix} \cos\theta & \sin\theta & 0 \\ -\sin\theta & \cos\theta & 0 \\ 0 & 0 & 1 \end{pmatrix} \cdot \begin{pmatrix} x'_r \\ y'_r \\ z'_r \end{pmatrix}. \tag{14}$$

Therefore, after simplification, the rotation angle of the x_Q and y_Q axes can be written as,

$$\varphi_x = \arctan(-\frac{z'_Q}{x'_Q}) = \arctan(\frac{\cos\theta \cdot \sin\alpha}{\cos\alpha \cdot \cos^2\theta + \sin^2\theta}) \tag{15}$$

$$\varphi_y = \arctan(\frac{z'_Q}{y'_Q}) = \arctan(\frac{\sin\theta \cdot \sin\alpha}{\cos\alpha \cdot \sin^2\theta + \cos^2\theta}). \tag{16}$$

When α is small enough, the higher-order terms of φ_x and φ_y can be ignored. Then, the formula (15) and (16) can be approximate as,

$$\varphi_x \approx \cos\theta \cdot \alpha, \quad \varphi_y \approx \sin\theta \cdot \alpha. \tag{17}$$

If the steering mirror rotates φ_x, the reflected light rotates $2\varphi_x$. Suppose the distance between the steering mirror and the QPD is L, the offset length on the QPD surface can be denoted as,

$$r_{rl} = L \cdot \tan(2\varphi_x) \approx 2L\cos\theta \cdot \alpha, \quad r_{ud} = L \cdot \tan(2\varphi_y) \approx 2L\sin\theta \cdot \alpha. \tag{18}$$

From the formula (18) we can conclude that the offset length is approximately proportional to the rotation angle of the steering mirror when the rotation angle is small. Theoretically, the improved DPS signal is also proportional to the small rotation angle.

Optics EXPRESS

With the experiment system in Fig. 6, we firstly set the laser intensity a high value. With high signal intensity, the influence of the equivalent current noise decreases. From the readout system, we know that the total voltage after photoelectric conversion is about 8.5 V. Then we change the rotation angle of the steering mirror and calculate the improved DPS signal of the left and right quadrants (D_{rl}). The relationship between them is shown in Fig. 8. The linear fitting curve is also drawn in the figure. Compared with Fig. 4, it can be seen that the experimental results agree well with the theory. When the offset length is small, D_{rl} is well proportional to the offset value. The linearity performance deteriorates with the increasing of the offset.

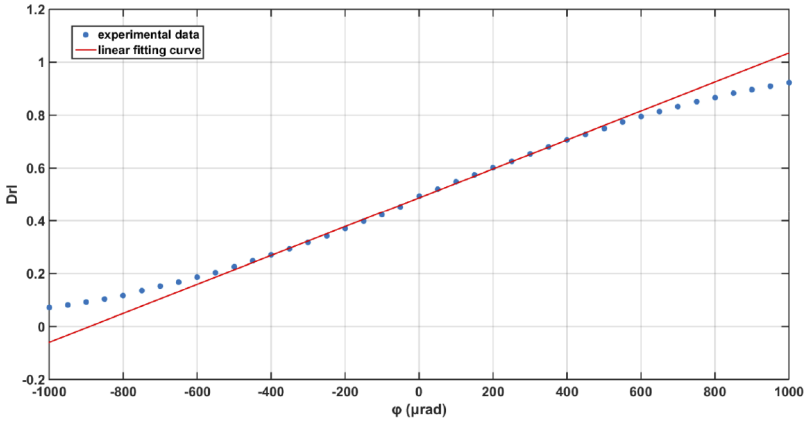

Fig. 8. The experimental result of the relationship between the rotation angle of the steering mirror and the improved DPS signal. The red curve is the linear fitting curve generate from the experimental data with small rotation angles.

We can also obtain the traditional DPS signal from the readout of the QPD. With the rotation angle ranging from -500 μrad to +500 μrad, the linear fitting coefficients of the DPS signals can be obtained. The coefficients here is obtained under high SNR condition. As the parameters of the experimental system except the light intensity will remain constant, the linear fitting coefficients will also be used in the following experiments to estimate the actual spot position. The estimated values from the linear fitting coefficients are denoted as $DPS_l(\varphi)$ and $D_{l,rl}(\varphi)$ respectively.

Theoretically, the improved DPS signal performs better than the traditional one in noisy environment. To verify such theory, we reduce the laser intensity with the attenuator and collect the traditional and the improved DPS signal of different rotation angles as $DPS(\varphi)$ and $D_{rl}(\varphi)$. The anti-noise performance is estimated by the root mean square value (RMS), which is denoted as,

$$RMS_{DPS} = \sqrt{\frac{1}{n}\sum_{\varphi(i)=-500\mu rad}^{500\mu rad}(DPS_l(\varphi(i)) - DPS(\varphi(i)))^2} \tag{19}$$

$$RMS_{D_{rl}} = \sqrt{\frac{1}{n}\sum_{\varphi(i)=-500\mu rad}^{500\mu rad}(D_{l,rl}(\varphi(i)) - D_{rl}(\varphi(i)))^2}, \tag{20}$$

where, n denotes the experiment times. With different laser intensity, the total voltage obtained from the readout system varies. The experimental results are shown in the Fig. 9. It can be concluded that the RMS error value increases with the decrease of the laser intensity while the RMS error value of the improved DPS signal is smaller than that of the traditional DPS signal. Therefore, the anti-noise performance of the improved DPS signal is better. It is proper to be used in the high-precision acquisition scheme.

Optics EXPRESS

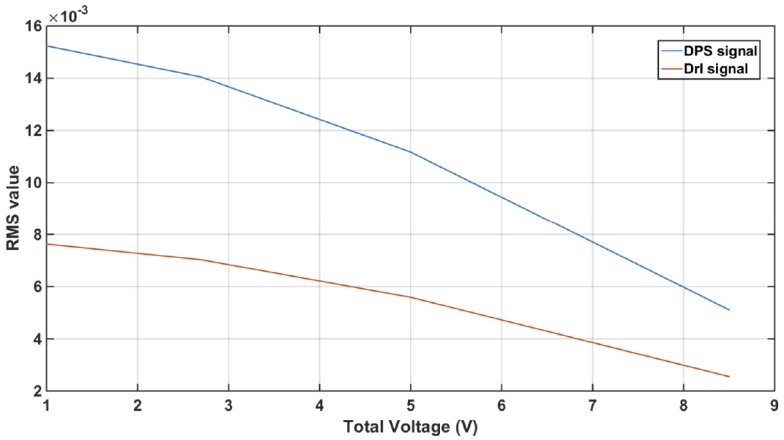

Fig. 9. The relationship between the RMS value and the total voltage obtained by the readout system. The red curve shows the relationship of the improved DPS signal while the blue curve presents the relationship of the traditional DPS signal.

3.2. Simulation results of the method

To verify the feasibility of the automatic QPD acquisition scheme, numerical simulation is carried out. For the Taiji program, the output laser power (P) is 1 W, the diameter of the telescope (D_{tel}) is 40 cm, the distance between two adjacent satellites (L) is 3×10^6 km, the diameter of the QPD (d_{QPD}) is 1 mm and the diameter of the laser spot on the QPD surface (d_{spot}) is set to 0.5 mm. These parameters are used in our simulation. As introduced in section 2.1, the half angle of the uncertainty zone is about 23.9 μrad in the acquisition phase while the target angle of the acquisition process (θ_{target}) should be 1 μrad. Considering some redundancy, we set θ_{uc}=25 μrad and the template gridding size θ_g=0.5 μrad in the simulation.

A dedicated imaging system is involved in QPD automatic acquisition scheme. The choice of the imaging system scale factors k_{ud} and k_{rl} greatly influence the acquisition precision. Here, we suppose that $k_{ud} = k_{rl}$=k. As introduced in section 2.2, the ASD of the QPD ECN is about 1.5 pA/$\sqrt{\text{Hz}}$. With a narrow band-pass filter, the noise current (I_{noise}) is approximately 1.5 pA. The receiving laser power depends on the relative position of the two satellites and the scanning strategy. For a fixed relative position, the maximum receiving laser power during scanning is denoted as P_{MAX}. For different relative positions, the minimum value of P_{MAX} is denoted as P_{min}. P_{min} increases with the decrease of the arc separation d. The decreasing of d will increase the number of scanning points (N) as well. Therefore, a tradeoff between SNR and the scanning time has to be made. When the satellite points to the correct direction, the minimum possible photo-current (I_{min}) is $\eta\cdot P_{min}$, where η=0.7 A/W. Therefore, the minimum resolvable distance of the QPD can be written as,

$$r_{\min} \approx 2d_{spot} \cdot \frac{I_{noise}}{I_{min}}. \tag{21}$$

As a result, for obtaining the acquisition precision of θ_{target}, the scale factor should fulfill,

$$k > \frac{r_{min}}{\theta_{target}} = \frac{2d_{spot}}{\theta_{target}} \cdot \frac{I_{noise}}{I_{min}}. \tag{22}$$

On the other hand, the nonlinearity of the improved DPS signal increases with the increase of the laser spot offset distance (as shown in the Fig. 3 and the Fig. 7). The nonlinearity property will cause deterioration of the acquisition precision. For guaranteeing enough precision, the

Optics EXPRESS

maximum offset distance should at least smaller than the radius of the laser spot. As a result, the imaging system scale factor should also fulfill,

$$k < \frac{d_{spot}/2}{\sqrt{2}\theta_{uc}} = \frac{\sqrt{2}d_{spot}}{4\theta_{uc}}. \tag{23}$$

It can be seen that the scale factor of the imaging system greatly influences the acquisition precision. It should guarantee enough minimum resolvable distance and the linearity property of DPS at the same time. Based on the above analysis, we finally set k=6.5 μm/μrad. From Fig. 4, it can be seen that the linear fitting coefficient of the improved DPS signal q_{rl}= q_{ud}≈2533 /m. Therefore, the incident angle can be derived from the detected DPS signal with the help of the formula (5).

Then a tradeoff between SNR of the detected data and the scanning time has to be made. The SNR of the receiving data increases with the increase of the stepping time (t_{step}) and the increase of the number of scanning points. However, increasing t_{step} and N will both increase the scanning time. For guarantee enough SNR for our algorithm, we finally set t_{step}=0.08 s and N=1100. Therefore, the scanning time for the maser scan is 88 s. Considering the time for satellite attitude adjustment and the time for laser propagation, the total scanning time for the whole acquisition process is within 220 s.

To improve SNR of the detected data and reduce the amount of effective data, the overall data collected by the QPD are firstly processed by the down sampling algorithm presented in formula (7)-(10). As presented in section 2.3, a template bank should be saved as a data base on the slave satellite before launch. A template records the down-sampled signal without noise for each scanning point, while each number m of the template corresponding to a specific location of the slave satellite. Figure 10 shows the examples of the template with slave satellite locating at different positions, which is denoted as ($\varphi_{m,yaw}$, $\varphi_{m,pitch}$).

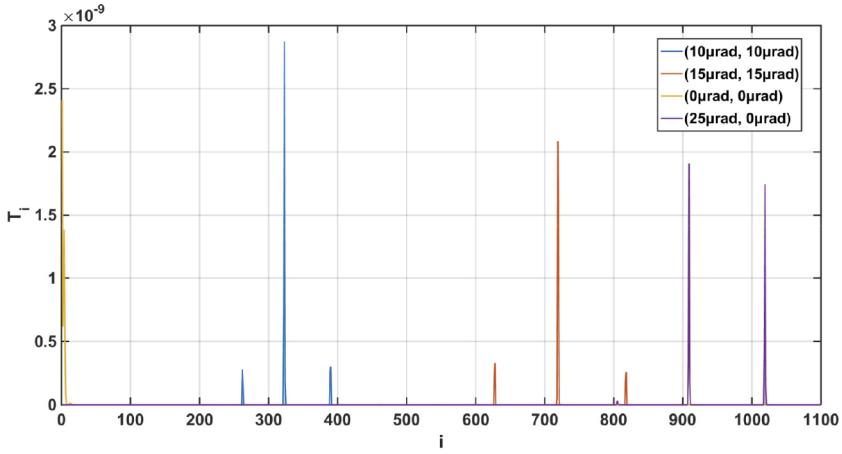

Fig. 10. Examples of the template with slave satellite locating at different positions.

Then, we add mutually independent Gaussian white noise (such as the one shown in Fig. 5(a)), whose ASD is 1.5 pA/$\sqrt{\text{Hz}}$, to each quadrant. We make the slave satellite position of (10μrad, 10μrad) as an example. With the help of the numerical simulation, the overall down-sampled data $S_{i,all}$ is presented in Fig. 11.

These data are match filtered by the template bank mentioned above. The values of the correlation C_m with respect to the pitch and the yaw directions are shown in Fig. 12. Then, we find out the point corresponding to the maximum C_m value. In Fig. 12, the position with the

Optics EXPRESS

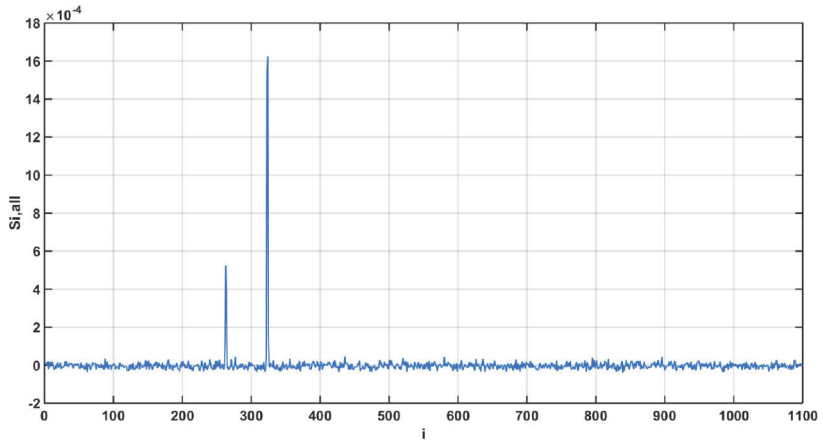

Fig. 11. The down-sampled value of $S_{i,,all}$. Where, the position of the slave satellite is (10μrad, 10μrad).

maximum value is (9.5μrad, 10.5μrad). In the relative template, we search for the maximum T_i value with i_{max}=324.

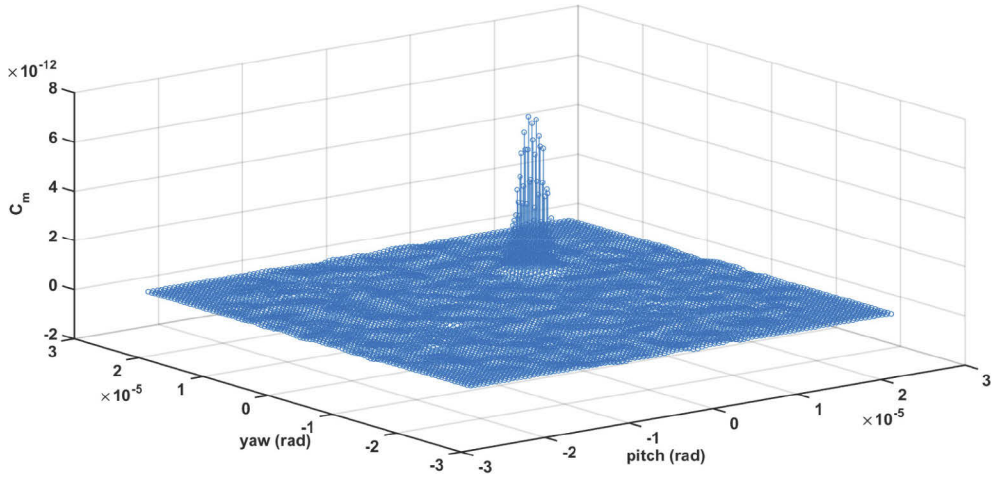

Fig. 12. Correlation result of C_m. Where, the position of the slave satellite is (10μrad, 10μrad).

With the help of the formula (11), the improved DPS signal can also be calculated. The $D_{i,rl}$ and $D_{i,ud}$ are not only depend on the slave satellite position ($\varphi_{m,yaw}$, $\varphi_{m,pitch}$) but also the slave satellite pointing direction ($\varphi_{s,yaw}$, $\varphi_{s,pitch}$). The incident angle is denoted as ($\varphi_{m,yaw}$-$\varphi_{s,yaw}$, $\varphi_{m,pitch}$-$\varphi_{s,pitch}$). In the simulation, we set the slave satellite pointing direction as (10μrad, 10μrad). Theoretically, the laser incident angle is (0 μrad, 0 μrad) at this time. The simulation results of $D_{i,rl}$ and $D_{i,ud}$ are respectively presented in Fig. 13 and Fig. 14. With $i = i_{max}$=324, the $D_{i,rl}$ and $D_{i,ud}$ value with the maximum SNR can be obtained. Then, we use the formula (5) to calculate the incident angle. The simulation result is (-0.0091 μrad, 0.057 μrad). Compared with the theoretical value, the measurement error is smaller than 1 μrad in both directions.

With the same process, we verify our automatic QPD acquisition scheme with various positions and pointing directions of the slave satellite. Table 1 shows the results. It can be seen that the

Optics EXPRESS

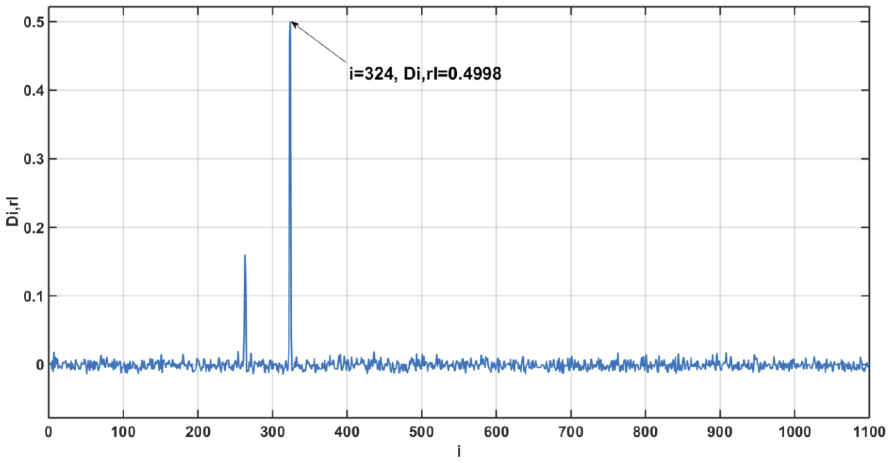

Fig. 13. The down-sampled value of $D_{i,,rl}$. Where, the position of the slave satellite is (10μrad, 10μrad), the pointing direction of the slave satellite is also (10μrad, 10μrad).

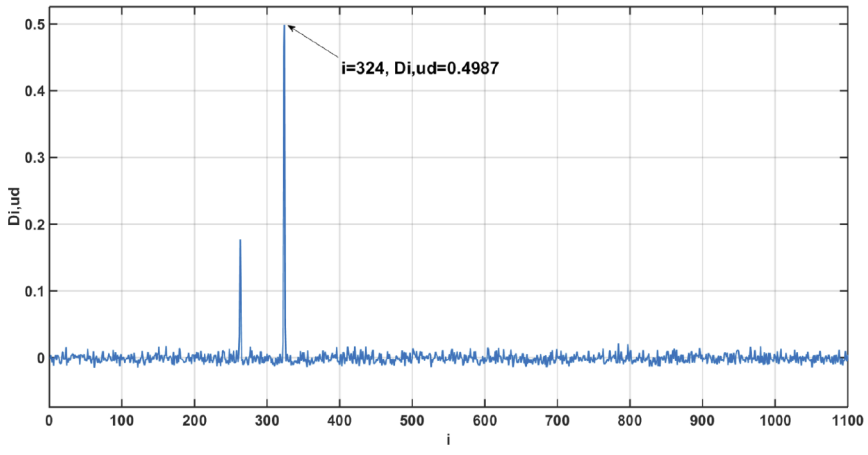

Fig. 14. The down-sampled value of $D_{i,,ud}$. Where, the position of the slave satellite is (10μrad, 10μrad), the pointing direction of the slave satellite is also (10μrad, 10μrad).

Optics EXPRESS

maximum angular deviation is less than 1 μrad. Therefore, the acquisition scheme can fulfill the precision requirement of the Taiji within 220 s.

Table 1. The results of various cases

$(\varphi_{m,yaw}, \varphi_{m,pitch})$ (μrad)	$(\varphi_{s,yaw}, \varphi_{s,pitch})$ (μrad)	Incident angle (μrad)	Simulation result (μrad)	Deviation Value (μrad)
(10, 10)	(10, 10)	(0, 0)	(−0.0091, 0.057)	(−0.0091, 0.057)
(10, 10)	(0, 10)	(10, 0)	(10.71, 0.85)	(0.71, 0.85)
(10, 10)	(10, 0)	(0, 10)	(0.15, 10.83)	(0.15, 0.83)
(0, 0)	(15, 15)	(- 15, - 15)	(- 14.76, - 14.96)	(0.24, 0.04)
(25, 0)	(0, 0)	(25, 0)	(24.15, - 0.57)	(- 0.85, −0.57)
(0, 25)	(0, 0)	(0, 25)	(0.14, 24.26)	(0.14, - 0.74)
(0, 10)	(15, 5)	(- 15, 5)	(- 15.07, 5.11)	(- 0.07, 0.11)
(17, 5)	(13, 2)	(4, 3)	(3.77, 2.75)	(- 0.23, −0.25)
(20, - 10)	(5, 5)	(15, - 15)	(15.74, - 14.41)	(0.74, 0.59)
(12, - 10)	(5, 7)	(7, - 17)	(7.25, - 16.33)	(0.25, 0.67)

4. Conclusion

In this paper, we present an automatic, high-speed and high-precision QPD acquisition scheme for the Taiji-like programs. With QPD being the only acquisition sensor, the scheme can overcome the heating problem of the CCD. The incoherent measurement method and a dedicated imaging system are involved in the scheme design. An improved DPS signal is developed for low SNR condition. The linearity performance and anti-noise performance of the signal are verified by an experiment. We also adopt down-sampling algorithm and match filter algorithm to improve the acquisition precision. Numerical simulation is used to test the performance of the scheme. The simulation results show that: the precision of the automatic QPD acquisition scheme can reach 1 μrad, which is the requirement of the Taiji, and the total acquisition time is within 220 s.

Funding. Chinese Academy of Sciences (XDA1501800003, XDA1502070304, XDA1502070902).

Disclosures. The authors declare no conflicts of interest.

References

1. B. P. Abbott, R. Abbott, T. D. Abbott, M. R. Abernathy, F. Acernese, and K. Ackley, "Observation of gravitational waves from a binary black hole merger," Phys. Rev. Lett. **116**(6), 061102 (2016).
2. K. Danzmann and A. Ruediger, "LISA technology concept, status, prospects," Classical Quantum Gravity **20**(10), S1–S9 (2003).
3. D. Cyranoski, "Chinese gravitational-wave hunt hits crunch time," Nature **531**(7593), 150–151 (2016).
4. W. Hu and Y. Wu, "The Taiji Program in Space for Gravitational wave physics and the nature of Gravity," Nat. Sci. Rev. **4**(5), 685–686 (2017).
5. Y. Wu, "Space Gravitational Wave Detection in China," Presentation to 1st eLISA Consortium Meeting, APC Paris, Oct. 22–23, 2012 (available at http://www.apc.univparis7.fr/APC/Conferences/First_eLISA_Consortium_Meeting/Expose_files/China_YLWU.ppt).
6. Z. Luo, Y. Wang, and Y. Wu, "The Taiji program: A concise overview," Progress of Theoretical and Experimental Physics. (2020).
7. M. Perryman, "The ESA-L3 Gravitational Wave Mission Gravitational Observatory Advisory Team Final Report," Technique Report. (2016).
8. X. Gong, S. Xu, S. Bai, Z. Cao, G. Chen, Y. Chen, and Z. Zhou, "A scientific case study of an advanced LISA mission," Classical Quantum Gravity **28**(9), 094012 (2011).
9. J. Luo, L. Chen, H. Duan, Y. Gong, S. Hu, J. Ji, and Z.-B. Zhou, "TianQin: a space-borne gravitational wave detector," Classical Quantum Gravity **33**(3), 035010 (2016).
10. P. Bender, "2001 LISA laser interferometer space antenna: a cornerstone mission for the observation of gravitational waves," ESA-SCI **11**, (2000).
11. LISA group member, "LISA pathfinder technical problem discussion," in Albert Einstein Institute (Hannover) group meeting (2016).

Optics EXPRESS

12. B. S. Sheard, G. Heinzel, K. Danzmann, D. A. Shaddock, W. M. Klipstein, and W. M. Folkner, "Intersatellite laser ranging instrument for the GRACE follow-on mission," J. Geod. **86**(12), 1083–1095 (2012).
13. F. Ales, P. F. Gath, U. Johann, and C. Braxmaier, "Modeling and simulation of a laser ranging interferometer acquisition and guidance algorithm," J. Spacer. Rockets **51**(1), 226–238 (2014).
14. C. Mahrdt, "Laser link Acquisition for the GRACE Follow-On Laser Ranging Interferometer," Doctoral thesis, Albert Einstein Institute. (2014).
15. F. Ales, P. F. Gath, U. Johann, and C. Braxmaier, "Line of sight alignment algorithms for future gravity missions," in *AIAA Guidance, Navigation, and Control Conference*. P. 0094 (2015).
16. Z. Luo, Q. Wang, C. Mahrdt, A. Goerth, and G. Heinzel, "Possible alternative acquisition scheme for the gravity recovery and climate experiment follow-on-type mission," Appl. Opt. **56**(5), 1495 (2017).
17. X. Wang, D. Xu, M. Tan, and Y. Liu, "A novel alignment method based on the four-quadrant photo electric detector," Transducer and Microsystem Technol. **25**(7), 11–14 (2006).
18. X. Tang, Y. Li, J. Liu, and K. Liang, "Alignment and Micro-Displace Measurement with Four-Quadrant Photo-Detector by System Modeling," Chin. J. Laser **36**(3), 746–751 (2009).
19. A. Joshi, J. Rue, and S. Datta, "Low-noise large-area quad photoreceivers based on low-capacitance quad InGaAs photodiodes," IEEE Photonics Technol. Lett. **21**(21), 1585–1587 (2009).
20. F. Guzman Cervantes, J. Livas, R. Silverberg, E. Buchanan, and R. Stebbins, "Characterization of photoreceivers for LISA," Class. Quantum Grav. **28**(9), 094010 (2011).